Hindawi
Shock and Vibration
Volume 2024, Article ID 9783415, 1 page
https://doi.org/10.1155/2024/9783415

Retraction

Retracted: Research on Temporal and Spatial Distribution Characteristics of Microseismic Events of Slip-Type Rockburst

Shock and Vibration

Received 23 January 2024; Accepted 23 January 2024; Published 24 January 2024

This article has been retracted by Hindawi following an investigation undertaken by the publisher [1]. This investigation has uncovered evidence of one or more of the following indicators of systematic manipulation of the publication process:

(1) Discrepancies in scope

(2) Discrepancies in the description of the research reported

(3) Discrepancies between the availability of data and the research described

(4) Inappropriate citations

(5) Incoherent, meaningless and/or irrelevant content included in the article

(6) Manipulated or compromised peer review

The presence of these indicators undermines our confidence in the integrity of the article's content and we cannot, therefore, vouch for its reliability. Please note that this notice is intended solely to alert readers that the content of this article is unreliable. We have not investigated whether authors were aware of or involved in the systematic manipulation of the publication process.

Wiley and Hindawi regrets that the usual quality checks did not identify these issues before publication and have since put additional measures in place to safeguard research integrity.

We wish to credit our own Research Integrity and Research Publishing teams and anonymous and named external researchers and research integrity experts for contributing to this investigation.

The corresponding author, as the representative of all authors, has been given the opportunity to register their agreement or disagreement to this retraction. We have kept a record of any response received.

References

[1] K. Xu, L. Song, W. Song et al., "Research on Temporal and Spatial Distribution Characteristics of Microseismic Events of Slip-Type Rockburst," *Shock and Vibration*, vol. 2022, Article ID 2262401, 15 pages, 2022.

Hindawi
Shock and Vibration
Volume 2022, Article ID 2262401, 15 pages
https://doi.org/10.1155/2022/2262401

Research Article

Research on Temporal and Spatial Distribution Characteristics of Microseismic Events of Slip-Type Rockburst

Kun Xu,[1] **Leibo Song**,[2,3] **Wenjie Song**,[1] **Jiangtao He**,[4] **Liping Li**,[1] **Ge Yan**,[5] **Qin Chen**,[5] **and Gang Wang**[2,3]

[1]*Wuhan Huike Quality Testing Co.,Ltd, Wuhan 430050, China*
[2]*School of Civil Engineering, Shaoxing University, Shaoxing 312000, China*
[3]*Key Laboratory of Rock Mechanics and Geohazards of Zhejiang Province, Shaoxing University, Shaoxing 312000, China*
[4]*China Gezhouba Group No. 1 Engineering Co., Ltd, Yichang 443000, China*
[5]*Wuhan Hanyang Municipal Construction Group Co., Ltd, Wuhan 430050, China*

Correspondence should be addressed to Leibo Song; song_leibo@163.com

Received 23 April 2022; Revised 12 June 2022; Accepted 29 June 2022; Published 16 July 2022

Academic Editor: Bangbiao Wu

Based on the microseismic monitoring data of underground cavern of Shuangjiangkou Hydropower Station, the internal relationship between rockburst and microseismic events is analyzed and the occurrence mechanism of slip-type rockburst in underground cavern of Shuangjiangkou Hydropower Station is analyzed through the change of microseismic monitoring *b* value to warn the risk level of rockburst. The results show that microseismic events are closely related to excavation activities, and the change of *b* value reflects the rockburst risk level. The smaller the *b* value of microseismic events is, the more large magnitude events is and the greater the possibility of rockburst is. The slip-type rockburst was mainly affected by structural plane; it is due to the accumulation of elastic strain energy at the structural plane and the sudden release under the action of unloading or disturbance, driving the block on the structure surface fast slide, mainly manifested as the sliding of large blocks of surrounding rock, and forming a "V" shape pit blasting or cuneate blasting crater, as well as destruction with crackle. Compared with the strained rockburst, the damage is more serious. The research results can provide reference for rockburst prediction and prevention in similar deep rock engineering.

1. Introduction

With the rapid development of China's national economic construction, the development of underground resources and space is also going deep [1]. The increase of resource mining depth makes the geological environment more complex. Under the complex geomechanical environment of "three highs and one disturbance" in the deep, engineering disasters are increasing day by day. Among them, the fault slip-type rockburst will cause huge damage and serious consequences to deep underground engineering and mining engineering [2, 3]. In particular, the excavation of deep underground caverns (roadways, tunnels, diversion tunnels, etc.) often needs to overcome difficulties such as high ground stress and complex geological structures, and rockburst is more serious under high-stress conditions [4]. Rockburst is easy to occur not only in hard and complete surrounding rock but also in rock mass with discontinuous geological structure. When certain lithologic conditions and stress conditions are met, the sudden dislocation and slip of discontinuous surface (such as joints and faults) will induce rockburst. The former is called strain rockburst and the latter is called fault slip-type rockburst [5]. The occurrence process of fault slip-type rockburst is similar to that of shallow earthquake. It is caused by the sudden shear instability of fault or structural plane, which will have a strong destructive effect on the surrounding rock. It is of great theoretical significance and engineering value to study the prediction and prevention of fault slip-type rockburst during blasting excavation of deep-buried caverns.

Affected by blasting excavation or mechanical disturbance, a large number of primary fractures in the natural rock mass expand and penetrate, and the elastic wave that can be received by the sensor is released during the fracture process. It is usually called microseism (MS) in the engineering field, and the microseismic signal contains a large amount of fracture information [6]. Therefore, in order to accurately monitor the precursor characteristics of rock mass deformation and failure to achieve advanced prediction and prevention, microseismic monitoring technology, as a safe and effective monitoring method, is widely used in tunnel excavation engineering. For example, Yu Qun et al. [7] used a digital multichannel microseismic monitoring system to monitor the rockburst of diversion tunnel #3 in real time for 24 hours. Through a large amount of microseismic monitoring data, the failure mechanism of dynamic crack propagation in the nucleation process of macroscopic instability rockburst was studied, including the initiation, development, propagation, shear zone formation, and coalescence. Dai et al. [8] studied the temporal and spatial distribution characteristics of microseismic events during the excavation of the underground powerhouse of the Houyan Hydropower Station, established the correlation between microseismic events and blasting construction, and used the FLAC3D program to simulate and verify. Li et al. [9] constructed a rockburst microseismic monitoring system for the underground powerhouse of Huanggou Pumped Storage Power Station. The spatiotemporal characteristics of microseismic activities during the monitoring period were analyzed, and the potentially dangerous areas of rockburst were identified and delineated. Guo [10] proposed a first-arrival picking method of effective signals for microseismic monitoring based on UNet++ network, which can significantly improve the accuracy and efficiency of microseismic time-difference source location. Zhang [11] studied the basic characteristics of MS events in heading face based on a running vibration signal acquisition system, including the occurrence position, main frequency range, maximum amplitude (MA) range, event duration, and relationship with geological structure. Ma et al. [12] studied the fracture and instability of rocks by analyzing the microseismic signals. Wang [13] built the ESG microseismic monitoring system on the driving face of 8005 transportation roadway of Wuyang Coal Mine to carry out a real-time, continuous, and omnidirectional dynamic state monitoring. In this way, the characteristics of time-frequency evolution and energy distribution of the acquired signals are systematically analyzed, and the location of the roadway microseismic events is studied. Jiang et al. [14] put forward the Local Energy Release Rate (LERR) to simulate the conditions causing rockburst. The results showed that LERR can satisfactorily predict the intensity of a rockburst and the depth of the outburst pit. Li et al. [15] constructed a high-precision microseismic monitoring system in two typical underground powerhouse caverns with different in situ stress levels and analyzed the b value and time variation microseismic characteristics of the large deformation of surrounding rock. Yang et al. [16] carried out the application research of microseismic monitoring technology in deep mines. The research results provided a new technical means for the prediction of mine roadway and pillar damage. Lei et al. [17] applied microseismic monitoring technology to the dam concrete monitoring of Guanyinyan Hydropower Station and analyzed the crack development process of dam concrete. Zhang et al. [18–20] successfully applied the microseismic monitoring technology to monitor the rockburst process in the diversion tunnel of Jinping II Hydropower Station in real time. Tao et al. [21] studied and applied the microseismic monitoring technology in the Han-Ji-Wei project, which provided a valuable reference for rock mass stability analysis in the construction of the Qinling super-long water conveyance tunnel. Xu et al. [22, 23] used microseismic monitoring technology to monitor and analyze the stability of surrounding rock during the excavation of underground caverns of Houziyan Hydropower Station in real time. Dai et al. [24] studied the failure evolution mechanism of surrounding rock under the disturbances of excavation and unloading of the underground powerhouse on the left bank of Baihetan Hydropower Station through microseismic monitoring technology. Li et al. [25–27] studied and analyzed the failure mode and formation mechanism of surrounding rock during the excavation of the underground powerhouse cavern group on the right bank of Wudongde Hydropower Station by means of microseismic monitoring technology. It showed that the temporal and spatial distribution law of microseism can well reflect the impact of underground powerhouse construction dynamics on surrounding rock disturbance.

The existing research is mainly based on microseismic monitoring technology to monitor and warn the strain-type rockburst during underground cavern excavation, and there are very few studies on the frequency and characteristics of slip-type rockburst microseismic events. In this paper, taking the underground powerhouse on the left bank of Shuangjiangkou Hydropower Station as the research background, a three-dimensional microseismic monitoring system is constructed. By collecting the frequency of microseismic events and analyzing the characteristics of microseismic events, combined with the fault slip-type rockburst phenomenon in the underground powerhouse of Shuangjiangkou, the internal relationship between rockbursts and microseismic events is discussed, and the mechanism of slip-type rockburst is revealed, which can provide a certain reference for other similar projects.

2. Engineering Background

The Shuangjiangkou Hydropower Station project is a first-class large (1) type project. The main buildings of the hub are Grade 1 buildings and the secondary buildings are Grade 3 buildings. The pivotal project is composed of barrage dam, water diversion and power generation system, flood releasing structures, and so forth. The barrage dam is a soil core rockfill dam with a total volume of about 44 million m^3, its dam height is 312 m, and the dam crest elevation is 2510 m. The flood releasing structures of the hub include tunnel spillway, straight slope spillway tunnel, shaft spillway tunnel, and reservoir emptying tunnel. The tunnel spillway,

straight slope spillway tunnel, and reservoir emptying tunnel are arranged on the right bank, while the shaft spillway tunnel is arranged on the left bank. The water diversion and power generation system is arranged on the left bank and the powerhouse is located underground of the left bank. Four vertical shaft Francis turbine generator units are installed in the powerhouse, and the layout patterns of "single machine, single pipe water supply" and "two machines, one room and one tunnel" are adopted.

The water diversion and power generation building on the left bank consists of the underground powerhouse system on the left bank (including main and auxiliary powerhouses, installation room, main transformer chamber, and tailrace surge chamber), water inlet, pressure pipes, and two tailrace tunnels. The underground powerhouse is arranged in the mountain upstream of the dam axis of the left dam abutment. The main and auxiliary powerhouses, the main transformer chamber and the tailrace surge chamber, are arranged in parallel, as shown in Figure 1. The longitudinal axis direction of the powerhouse is N10° W, the horizontal buried depth is about 400 m, and the vertical buried depth ranges from 320 m to 500 m.

According to the field geological data, the horizontal buried depth of the underground powerhouse ranges from 400 m to 640 m, the vertical buried depth ranges from 320 m to 500 m, and the maximum principal stress ranges from 20 MPa to 40 MPa. The maximum principal stress at the 400 m vertical buried depth measured by drilling is 37.82 MPa, its azimuth angle is 331.6°, and the inclination angle is 46.8°. The lithology of the exposed stratum in the power generation building area is mainly Kerin granite complex-Muzudu porphyritic biotite potassium feldspar granite in early period of Yanshan. The saturated compressive strength is generally above 60 MPa. The acoustic wave velocity of rock mass is generally 4900~5400 m/s. The surrounding rock mass of the underground powerhouse has good integrity, local dykes are developed, and the main structural planes are secondary small faults and joint fissures. The crack spacing is large, mostly greater than 1 m. The extension length of cracks ranges from 2 m to 3 m, and a few of them can reach 5 m to 6 m or longer. The crack surface is fresh, undulating and rough, and closed without filling. The underground powerhouse of Shuangjiangkou Hydropower Station has the engineering characteristics of "long span, high side wall, and high ground stress." The surrounding rock is prone to unstable failure, especially affected by high ground stress. Rockburst disasters occur frequently, and the potential risk of construction is high. It is urgent to carry out in-depth research on the precursory characteristics and early warning of surrounding rock fracture and failure under the influence of construction.

3. Construction of the Microseismic Monitoring System in Underground Powerhouse

3.1. Microseismic Monitoring System. Under the action of external stress, energy accumulation promotes the initiation and expansion of microcracks in rock materials. At the same time, with the rapid release and propagation of elastic waves

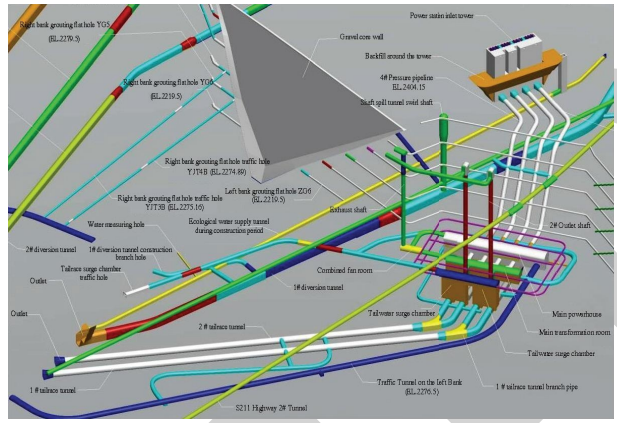

Figure 1: Layout of the buildings for diversion and power generation on the left bank.

Figure 2: Mainframe processing system, substations, and sensors of the microseismic monitoring system.

in adjacent rock mass, acoustic emission is generated. For large-scale rock mass engineering, it is also called microseism (MS). ESG microseismic monitoring system can predict the evolution law of microseismic activities. It is often used for the stability monitoring and analysis of rock or concrete engineering structures such as slopes, tunnels, mines, and dams. ESG microseismic monitoring system consists of hardware and software, as shown in Figure 2.

3.2. Microseismic Monitoring Scheme. According to the installation requirements of ESG microseismic monitoring system, combined with the on-site construction of power generation system of Shuangjiangkou Hydropower Station, the on-site layout scheme of microseismic system is determined as follows. In order to keep the system monitoring synchronized with the construction progress, the installation position needs to be adjusted dynamically according to the excavation. In terms of the construction tunnel, the sensors are arranged in sequence with a distance of about 50 m from front to back, with three sensors on the left, middle, and right, respectively. The first sensor at the top of the tunnel is installed at the front, about 40 m away from the tunnel work face, and the first sensors on both sides are at the same position, about 50 m away from the tunnel work face. The host processing system and the receiving substation are arranged together. The sensors and substations are connected by communication cables, and the substations are connected with the host processing system by optical fibers,

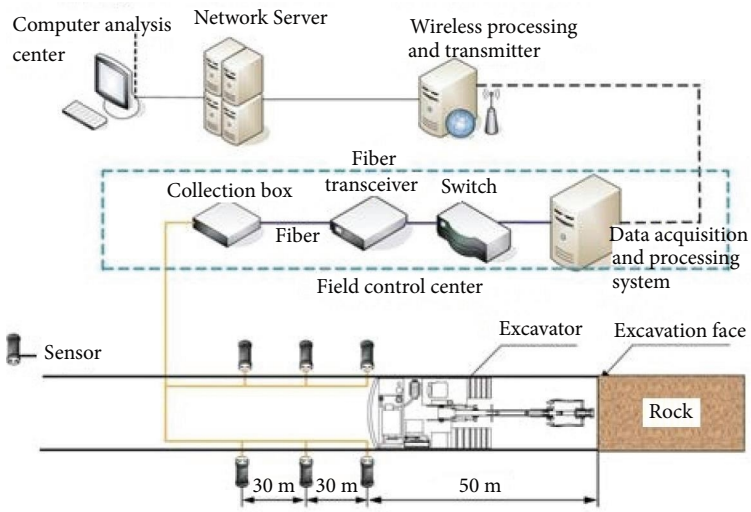

Figure 3: Layout of tunnel sensors.

as shown in Figure 3. For the three tunnels, in principle, sensors are dynamically adjusted and arranged in the top arch, side wall, and drainage gallery, as shown in Figure 4.

The accuracy of seismic source location is a prerequisite for effective microseismic monitoring in rock mass engineering. The location error is mainly restricted by factors such as sensor spatial location, sensor array mode, signal arrival time, rock mass wave velocity, and location method. The heterogeneity and complexity of rock mass structure lead to different requirements for microseismic positioning accuracy in different rock mass projects. Usually, the microseismic positioning accuracy of underground caverns in water resources and hydropower projects is less than 12 m (or even 10 m). The accurate measurement of rock mass wave velocity plays a vital role in microseismic positioning. Therefore, before the effective microseismic monitoring of the tailrace tunnel of Shuangjiangkou Hydropower Station is carried out, the wave velocity of surrounding rock mass in the tunnel must be accurately determined.

The entrance traffic tunnel of Shuangjiangkou Hydropower Station adopts the simplex method with good stability and high calculation accuracy to calculate the microseismic position, and the microseismic positioning error of surrounding rock mass of tailrace tunnel is reduced by optimizing the elastic wave velocity of rock mass. On December 10, 2017, six locations were selected in the sensor array space of the microseismic monitoring system of the incoming entrance traffic tunnel to carry out the artificial fixed-point knock test. According to the wave velocity range of the surrounding rock mass, the simplex method was used to calculate the location of the knock event in the range of 4800~5500 m/s. Compared with the actual knock location, the positioning error was calculated. When the elastic wave velocity of surrounding rock mass is 5100 m/s, the average positioning error is the smallest, it is 7.2 m, and each error is controlled within 10 m, which meets the positioning requirements of the microseismic monitoring system for underground caverns of the hydropower station.

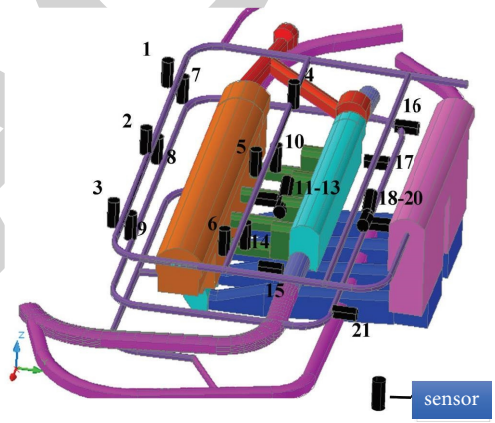

Figure 4: Network topology of the rockburst microseismic monitoring system in Shuangjiangkou underground cavern.

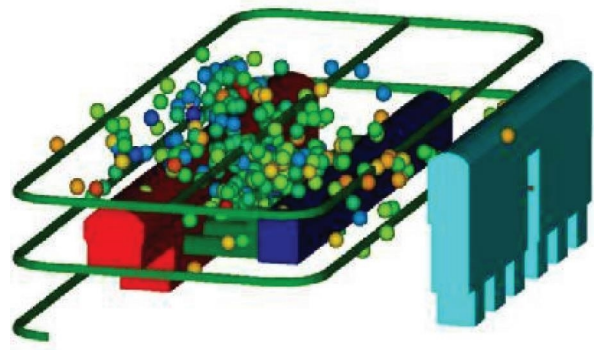

Figure 5: Microseismic monitoring of the underground powerhouse.

4. Analysis of Microseismic Activity Characteristics in the Underground Powerhouse

The rockburst grade of Shuangjiangkou Hydropower Station is determined by the moment magnitudes and the number of

Table 1: Determination method of the rockburst grade.

Options	None	Slight	Moderate	Relatively strong	Strong
Moment magnitude	−2.5 ~ −1.5	−1.5 ~ 0	0 ~ 1.0	1.0 ~ 2.5	> 2.5
Number of microseismic events	< 5	5 ~ 10	10 ~ 20	20 ~ 40	> 40
Determination of rockburst grade	The rockburst grade is comprehensively determined by the moment magnitudes and the number of daily microseismic events. When the actual situation is inconsistent with the table, the cross determination method is used. For example, ① the moment magnitude ranges from −2.5 to −1.5, the number of microseismic events reaches 5 to 10 times, and the rockburst grade is from none to slight; ② the moment magnitude ranges from 0 to 10, the number of daily microseismic events is 5 to 10 times, and the rockburst grade is from slight to moderate.				

daily microseismic events. Typical microseismic monitoring effects of Shuangjiangkou Hydropower Station are shown in Figure 5. For the abnormal increase phenomenon of microseismic events, the rockburst grade needs to be increased by one level [28]. The judgment standard is shown in Table 1.

4.1. Temporal Distribution Law of Microseismic Events. The microseismic monitoring of the entrance traffic tunnel began on January 1st, 2018, and ended on October 24th, 2018, with a total of 828 microseismic events detected, as shown in Figure 6. Among them, no construction was carried out from February 6th to March 6th, and there was no monitoring data. The number of microseismic events was relatively high from January 5th to January 25th and from March 22nd to April 12th. The number of microseismic events was the highest on January 20th, reaching 32 times. It is obvious that there were many microseismic events in the early stage of construction. There was no rockburst prediction data in the early stage, the excavation rate was fast, the support strength was low, and the surrounding rock was strongly disturbed by unloading. Therefore, there were many microseismic events and frequent rockbursts. In the later stage, the construction scheme was optimized according to the characteristics of rockbursts and the surrounding rock support was strengthened. It is found that the number of microseismic events was significantly reduced and the rockbursts were well controlled. From the explanation of rockburst mechanism, optimizing the construction scheme was to reduce the unloading or disturbance effect and the release of strain energy of surrounding rock, thereby reducing the risk of rockbursts [29–31]. Strengthening support was to improve the energy storage limit of surrounding rock and prevent the occurrence of rockbursts.

The moment magnitude distribution of microseismic events ranges from −2.0 to −0.5, as shown in Figure 7. According to the determination method of rockburst grade in Table 1, the entrance traffic tunnel is dominated by slight rockbursts, with 8 times of moderate rockbursts. However, from January 19, 2018, to January 20, 2018, the number of microseismic events increased from 3 times to 32 times, which may lead to relatively strong rockbursts.

The microseismic monitoring system of the main powerhouse was put into operation on July 19, 2018, and, by December 31, 2019, a total of 1,695 microseismic events were monitored, as shown in Figure 8. Among them, the number of daily microseismic events in 39 days was more than 10, the

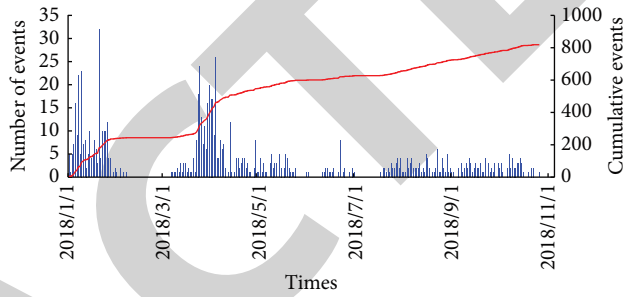

Figure 6: Time distribution of microseismic events in the traffic tunnel.

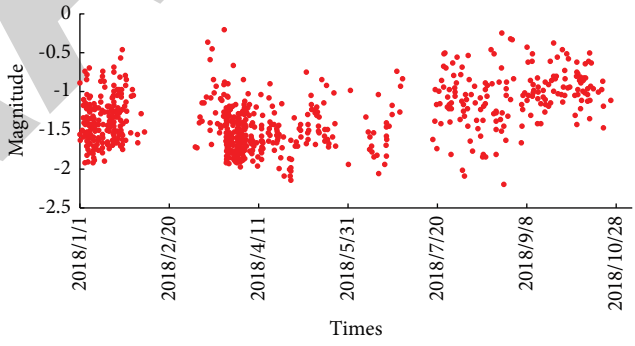

Figure 7: Relationship between magnitude and time of microseismic events in the traffic tunnel.

number of microseismic events on the remaining days was less than 10, and the maximum number of daily microseismic events was 19. By comparison, it is found that the number of microseismic events in 2018 was significantly higher than that in 2019. The height of the main powerhouse was 65.89 m. The main powerhouse was excavated in layers. During the early excavation, the unloading effect was strong and the energy was released more, so the number of microseismic events was more. At the same time, in the later stage, the excavation method was optimized, and the prevention and control of rockbursts were strengthened, so that the number of microseismic events was significantly reduced.

The moment magnitude distribution of microseismic events ranges from −2.5 to 0.5, as shown in Figure 9. According to the determination method of rockburst grade in Table 1, the main powerhouse was dominated by slight rockbursts, with 46 times of slight or moderate rockbursts,

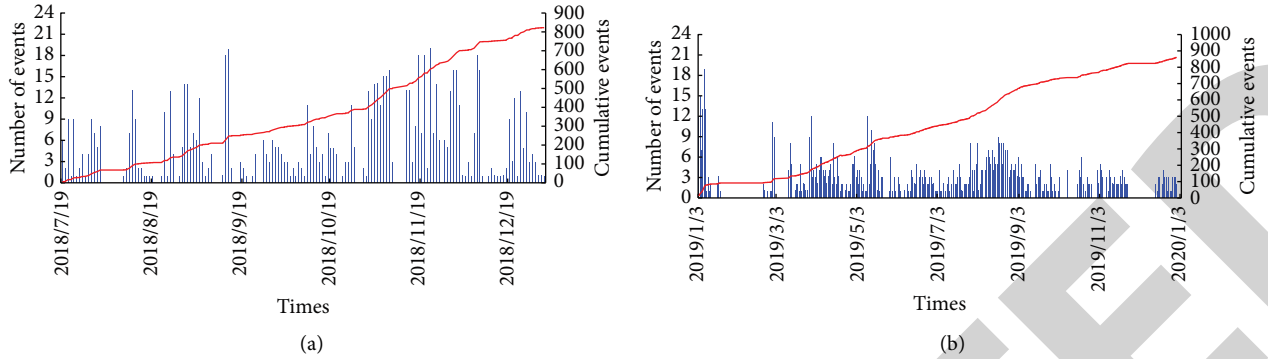

Figure 8: Time distribution of microseismic events in the main powerhouse. (a) In 2018. (b) In 2019.

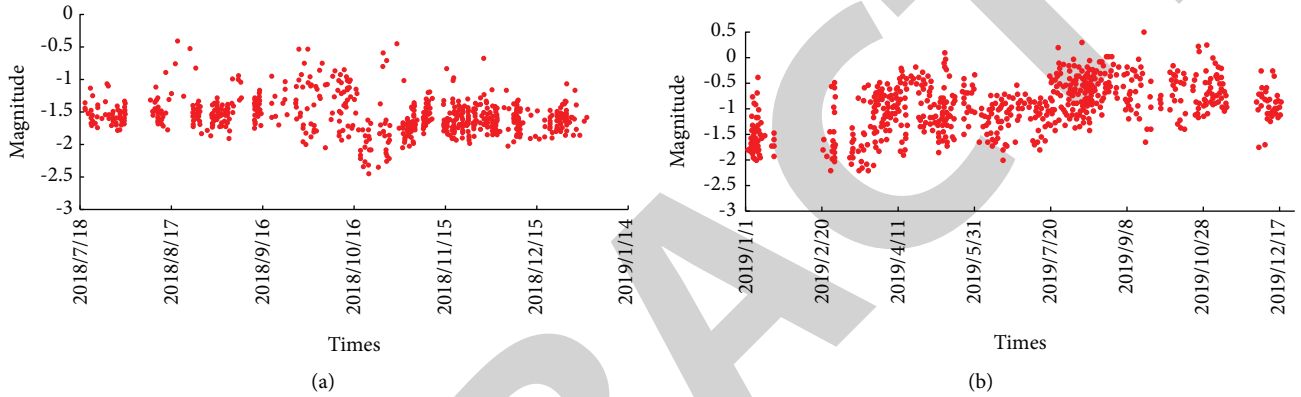

Figure 9: The relationship between the magnitude and time of microseismic events in the main powerhouse. (a) In 2018. (b) In 2019.

and no strong rockbursts occurred. Rockburst mainly occurred in November 2018.

The tailrace tunnel microseismic monitoring system has been in operation since November 15, 2019, and a total of 170 microseismic events had been monitored by December 31, 2019, as shown in Figure 10. Among them, the number of daily microseismic events in 4 days was more than 10, and the number of microseismic events on November 16, 2018, was the largest, reaching 16. The start date of tailrace tunnel construction was relatively late, the rockburst prevention and control measures were relatively mature, and the unloading and disturbance effects of surrounding rock were significantly reduced. Therefore, the number of microseismic events was generally small during tailrace tunnel excavation.

The distribution range of moment magnitude of microseismic events ranges from −2.5 to 0.7, as shown in Figure 11. On December 28th, 2019, the maximum moment magnitude of microseismic events was 0.7, which was a moderate rockburst moment magnitude. However, the number of microseismic events was less than 5 times, so it was judged as slight rockburst. The rockbursts in the tailrace tunnel were mainly slight rockbursts, with 4 times of slight-to-moderate rockbursts.

4.2. Spatial Distribution Law of Microseismic Events. In the spatial distribution diagram of microseismic events, a single

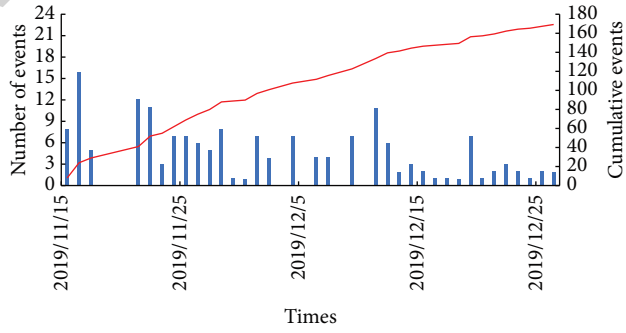

Figure 10: Time distribution of microseismic events in the tailrace tunnel.

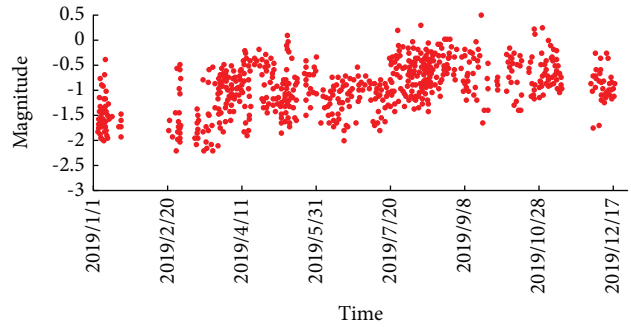

Figure 11: Relationship between magnitude and time of microseismic events in the tailrace tunnel.

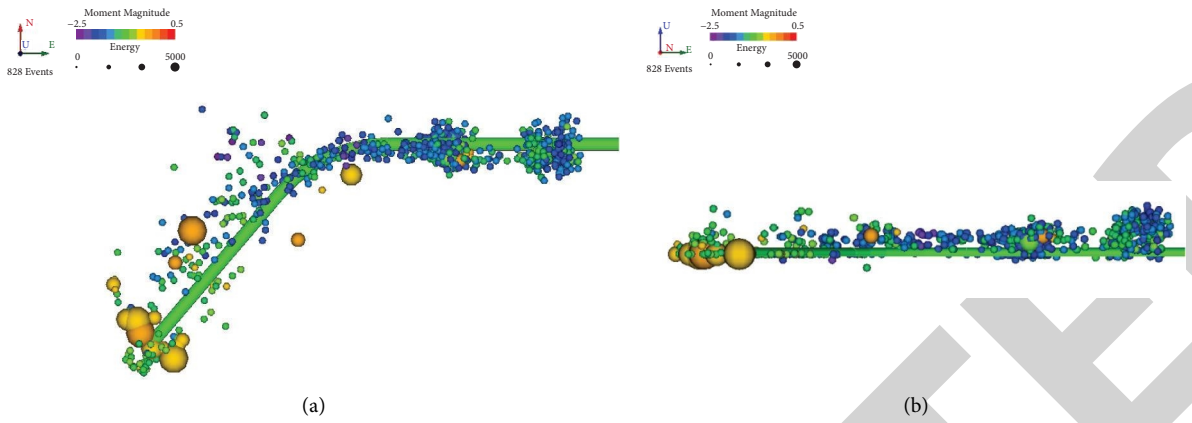

(a) (b)

Figure 12: Spatial distribution of microseismic events in the traffic tunnel. (a) Planform. (b) Left view.

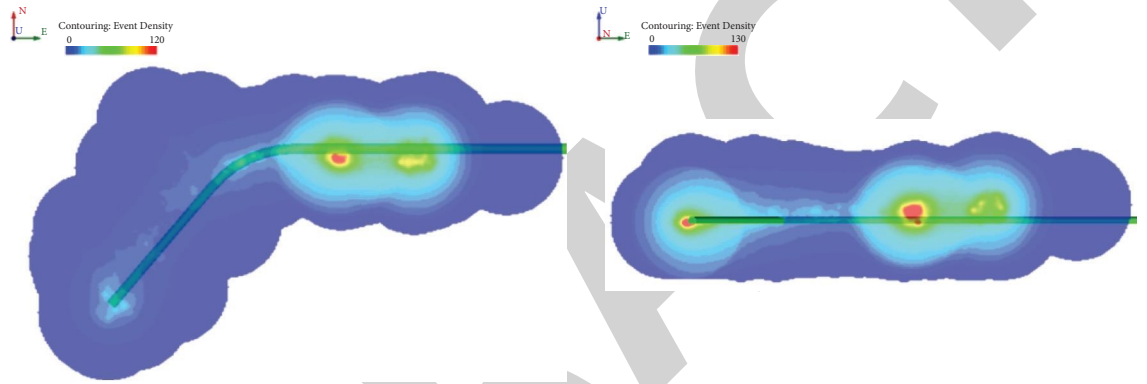

(a) (b)

Figure 13: Density cloud chart of microseismic events in the traffic tunnel. (a) Planform. (b) Left view.

microseismic event is represented by a sphere, and its matrix magnitude is represented by the depth of the sphere color. As the color of the sphere becomes darker, the moment magnitude is higher. The energy of microseismic events is expressed by the volume of the sphere. With the increase of the volume of the sphere, the moment magnitude increases. The spatial distribution law of microseismic events in the entrance traffic tunnel from January 1, 2018, to October 24, 2018, is shown in Figure 12. Among them, the areas with the largest number of events are (traffic tunnel) 0 + 391~0 + 414 m and (traffic tunnel) 0 + 516~0 + 563 m, which are prone to rockbursts. There are not many microseismic events in the area of (traffic tunnel) 0 + 0~0 + 30 m, but there are many high-energy and large-magnitude events, which is also an area prone to rockbursts.

The density nephogram of microseismic events is divided into five colors, namely, dark blue, blue, green, yellow, and red. The dark blue area is the undisturbed area, regardless of the possibility of rockburst. In addition, from blue to red, the density of microseismic events gradually increases with the deepening of color. The probability of rockburst in the blue area is 0% to 25%, which is a relatively safe area. The probability of rockburst in the green area is 25% to 50%, which is a general safety area. The probability of rockburst in the yellow area is 50% to 75%, which is a dangerous area. The probability of rockburst in the red area is 75% to 100%, which is an extremely dangerous area. Because the red area is an extremely dangerous area, it is generally predicted as the source area of rockburst. Figure 13 shows the density nephogram of microseismic events in the entrance traffic tunnel. The possible areas of rockbursts are (traffic tunnel) 0 + 391~0 + 414 m, (traffic tunnel) 0 + 0~0 + 30 m, and (traffic tunnel) 0 + 516~0 + 563 m.

The spatial distribution law of microseismic events in the main powerhouse is shown in Figure 14. The area with the largest number of events is (powerhouse) 0 + 96~0 + 136 m, followed by (powerhouse) 0 + 176~0 + 208 m. Among them, in 2018 and 2019, the number of microseismic events in (powerhouse) 0 + 96~0 + 136 m was accumulated, indicating that the stress was concentrated and there was more energy accumulation here. According to the geological data of Shuangjiangkou, a lamprophyre vein is developed near K0 + 135 m and extends to the downstream side wall near the end wall. The structural plane attitude is 225°∠72° and the width ranges from 30 cm to 60 cm. The rock mass in the dyke zone is broken into blocks, and the fractured structure is compact and dry. This dyke intersects with the tunnel at a large angle. Affected by the structural plane, it is very easy to induce fault slip-type rockburst under the action of high-stress unloading. The monitoring shows that the probability of rockburst here is high. It can also be seen that the number

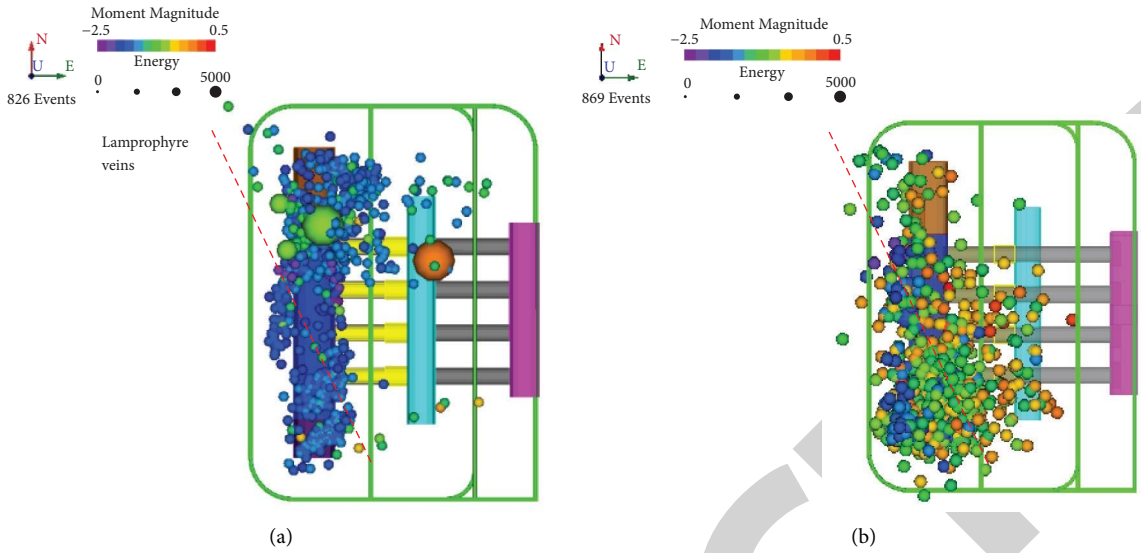

Figure 14: Spatial distribution of microseismic events in the main powerhouse. (a) In 2018. (b) In 2019.

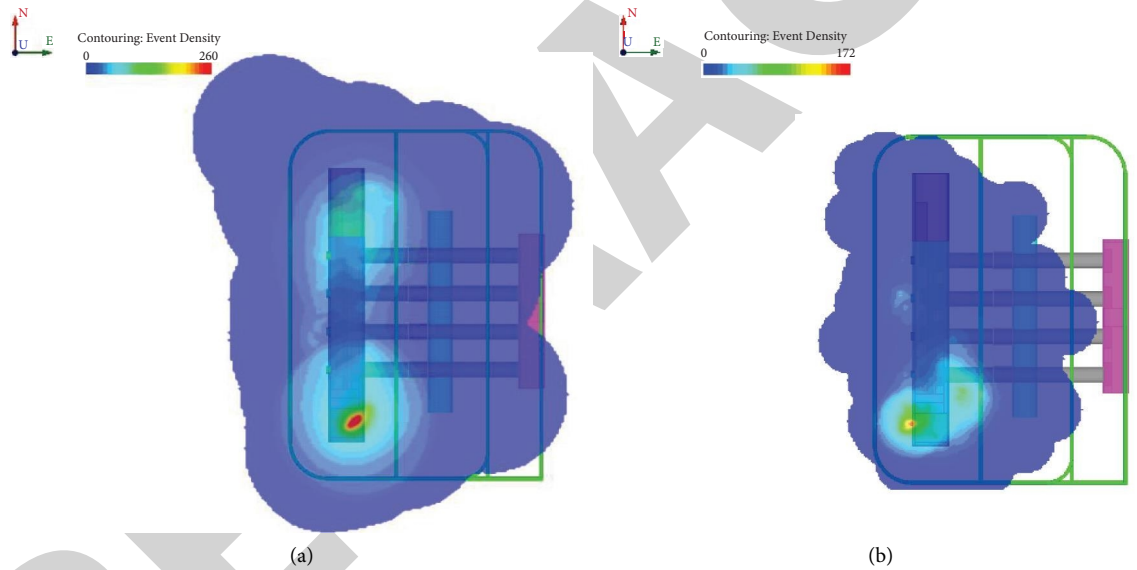

Figure 15: Density cloud map of microseismic events in the main powerhouse. (a) In 2018. (b) In 2019.

of microseismic events on the right side is more than that on the left side, which is mainly caused by the different stress on both sides.

Figure 15 shows the density nephogram of microseismic events in the main powerhouse, which is extremely consistent with the spatial distribution diagram of microseismic events. The rockburst areas are (powerhouse) 0 + 96–0 + 136 m and (powerhouse) 0 + 176–0 + 208 m.

The spatial distribution law of microseismic events in tailrace tunnel is shown in Figure 16. The area with the largest number of events is (2# tailrace) 0 + 500~0 + 600 m. This is the excavation area, indicating that the microseismic events are mainly concentrated near the tunnel face; that is, the rockburst mainly occurs at the tunnel work face. The excavation face is strongly subjected to unloading and disturbance effects, and the strain energy accumulated in the surrounding rock mass is suddenly released under unloading effect, resulting in the occurrence of rockburst events.

Figure 17 is the density nephogram of microseismic events in the tailrace tunnel, which is consistent with the spatial distribution diagram of microseismic events. The area of rockburst is (2# tailrace) 0 + 500~0 + 600 m. Comparing the entrance traffic tunnel and the main powerhouse, it is found that the tailrace tunnel has a smaller rockburst area, and the probability of rockburst is also small. This is mainly because the tailrace tunnel has not been excavated, the unloading or disturbance area of surrounding rock mass is small, and the monitoring data is less. It indicates that microseismic monitoring is closely related to excavation activities.

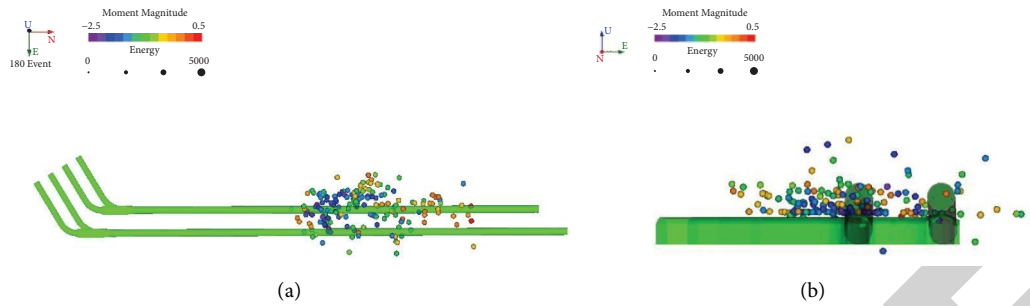

(a) (b)

Figure 16: Spatial distribution of microseismic events in the tailrace tunnels. (a) Planform. (b) Left view.

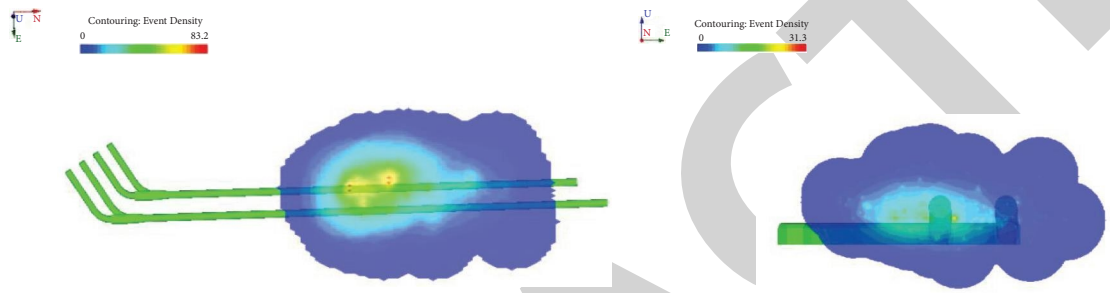

(a) (b)

Figure 17: Density cloud map of microseismic events in the tailrace tunnel. (a) Planform. (b) Left view.

4.3. Moment Magnitude Distribution Law of Microseismic Events. Moment magnitude and frequency of microseismic events and natural earthquakes follow the frequency-magnitude relationship introduced by Gutenberg–Richter (G-R formula).

$$\lg \cdot N = a - b \times M, \tag{1}$$

where M is the moment magnitude, N is the number of microseisms with a magnitude greater than or equal to M, and a and b are constants. The b value represents the proportional relationship between the numbers of large- and small-magnitude events. The smaller the b value is, the more large-magnitude events are. The change of b value can be used to reflect the change of stress field. The b value can reflect the source characteristics of microseismic activity. The b value of microseismic activity related to fault slip is relatively low, generally less than 0.8. The b value of microseismic activity caused by stress adjustment is usually between 1.2 and 1.5.

The moment magnitude-frequency curve of 828 microseismic events in the entrance traffic tunnel is shown in Figure 18. It can be seen that there are large deviations in the minimum and the maximum magnitudes. The deviation of the minimum magnitude is caused by the sensitivity of the monitoring system and the characteristics of small magnitude events. The farther the sensor array is, the smaller the sensitivity of microseismic monitoring system is and the larger the minimum moment magnitude of microseismic events is. The sampling deviation in the maximum magnitude event is due to the low frequency of large-magnitude microseismic events, resulting in incomplete samples of large-magnitude microseismic events. Therefore, the

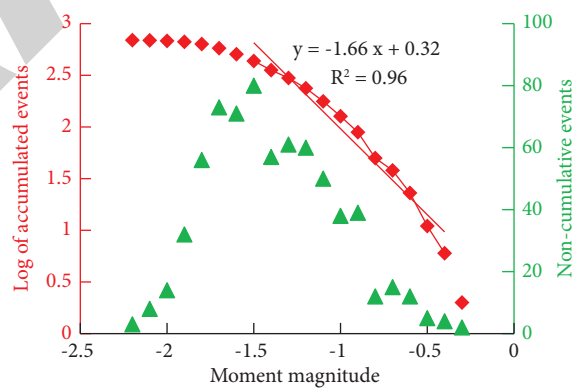

Figure 18: Moment magnitude-frequency curve of the traffic tunnel.

maximum and minimum magnitude thresholds should be set when calculating the b value. The minimum magnitude threshold is the peak point of the magnitude-noncumulative frequency curve, and the maximum magnitude threshold is the minimum value that deviates from the trend line on the magnitude-cumulative frequency curve. When the b value increases or changes slightly, the surrounding rock is relatively stable and the probability of rockburst is low. When the b value decreases significantly, it indicates that the damage in the rock mass is intensified and the probability of rockburst is high.

According to the above method, the moment magnitude-frequency curve of microseismic events in tailrace tunnel in Figure 19 and the moment magnitude-frequency

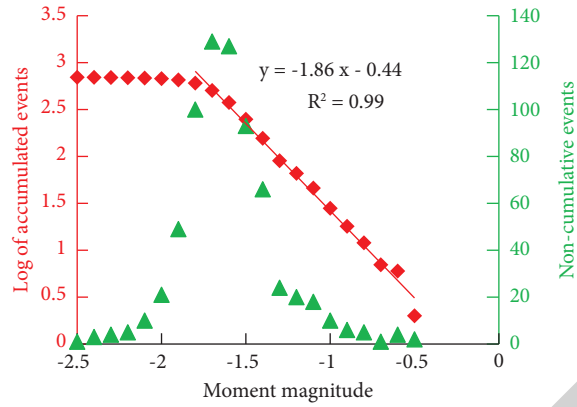

Figure 19: Moment magnitude-frequency curve of the tailrace tunnel.

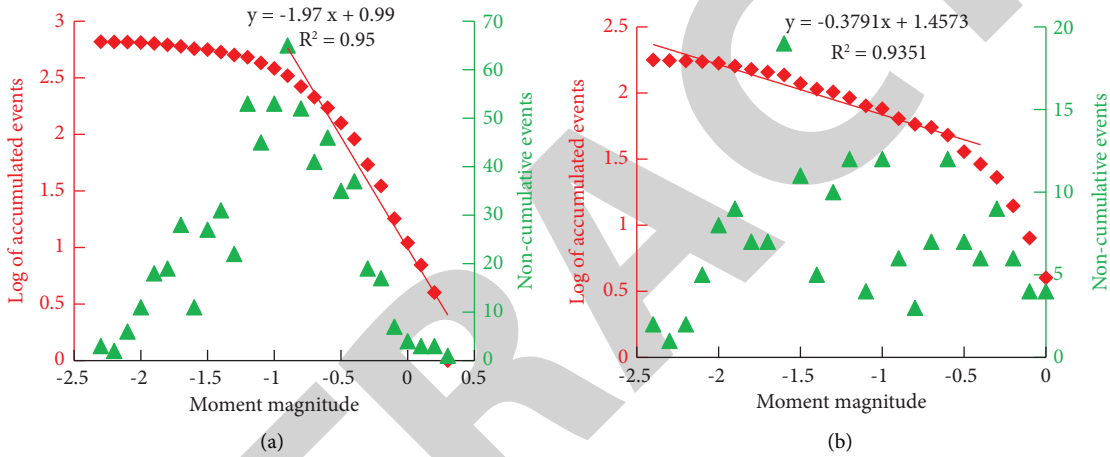

Figure 20: Moment magnitude-frequency curve of the main powerhouse. (a) In 2018. (b) In 2019.

curve of microseismic events in main powerhouse in Figure 20 are drawn. Combined with the time relationship diagram of moment magnitude of microseismic events, it can be obtained that the smaller the b value is, the more large-magnitude events are and the greater the possibility of rockburst is. Compared with the b value of microseismic events in the main powerhouse, it was 1.97 in 2019, which was higher than 1.86 in 2018. The probability of rockburst in 2019 was lower than that in 2018, which was consistent with the occurrence of rockburst on-site.

In conclusion, the b value can reflect the activity of microseismic events with different magnitudes. The change of b value can reflect the risk level of rockburst, which can be used as an important index to reflect the overall stability of surrounding rock in the area.

5. Analysis and Discussion on the Characteristics of On-Site Slip-Type Rockburst

5.1. Investigation of Slip-Type Rockburst in the Main (Auxiliary) Powerhouse. In the auxiliary powerhouse K0 + 180.6 m, it is found that the rocks are caving and accompanied by sound, as shown in Figure 21. A group of structural planes inclined to SW are developed on the upstream side, with an occurrence of 240°∠45° and spacing of 0.5~0.8 m. Affected by this group of structural planes, fault slip-type rockburst controlled by structural plane occurs on the upstream side, forming a wedge-shaped cavity. Strain-type rockburst occurs on the downstream side, and layered exfoliation pops up.

Acoustic emission signal and small stone pop-up sound are monitored in K0 + 010~K0 + 013 m section of pilot tunnel in the main powerhouse. The occurrence of the structural plane is 230~250°∠30–50°. It forms a natural shear-out structural plane with another group of 30°∠45° structural planes at the upstream side wall and spandrel, where moderate strength fault slip-type rockburst occurs during excavation (Figure 22.)

The V-shaped blasting pit can be seen in the upstream side wall vault of the pilot tunnel K0 + 100 m in the main powerhouse, and joint development can be seen at the same time. In the process of cavern excavation, the stress is redistributed, and the shear stress on the structural plane exceeds its friction, resulting in the shear failure of the surrounding rock along the structural plane and the ejection

Figure 21: Failure mode diagram of the auxiliary powerhouse.

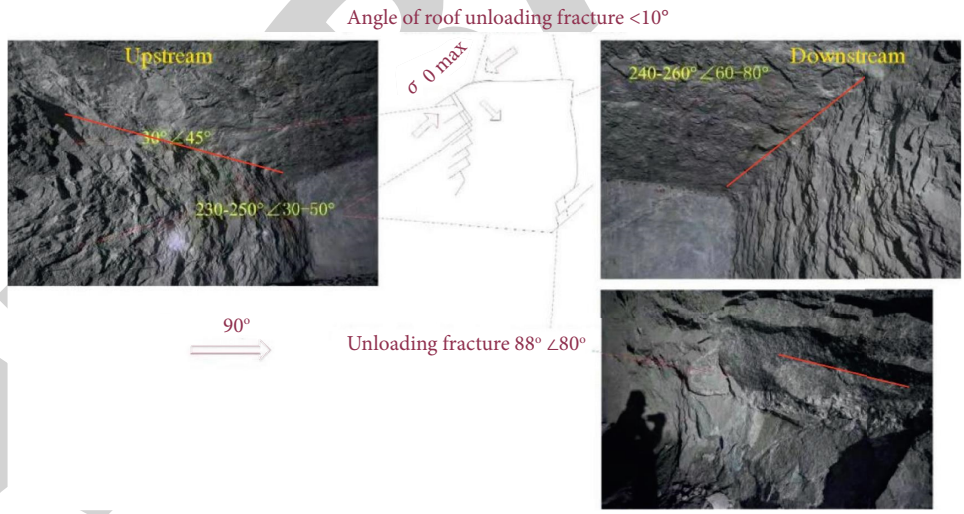

Figure 22: Deformation and failure of the surrounding rock in the K0 + 010.00–K0 + 013 m of the pilot tunnel.

of rock blocks along the structural plane, so that the fault slip-type rockburst is generated, as shown in Figure 23.

A lamprophyre vein is developed near K0 + 135 m of the main powerhouse, extending to the downstream side wall near the end wall. The occurrence of the structural plane is 225°∠72°, with a width of 30 cm to 60 cm. The rock mass in the dyke zone is broken into blocks, and the fractured structure is compact and dry. This dyke intersects with the tunnel at a large angle. Affected by the structural plane, the fault slip-type rockburst is induced under the action of high-stress unloading, as shown in Figure 24.

5.2. Investigation of Fault Slip-Type Rockburst in the Main Transformer Chamber. In the main transformer chamber, rocks can be seen falling at K0 + 70 m in the pilot tunnel, accompanied by rockburst sound, and a group of structural planes 240°∠61°, 250°∠48°, 260°∠53°, and 262°∠48° are developed on the upstream side, with spacing of 0.1~0.5 m. Excavation unloading induces large blocks at the structural plane to slide down, resulting in fault slip-type rockburst, as shown in Figure 25.

Wedge-shaped failure occurs in the downstream side wall and spandrel at K0 + 10 m of the main transformer

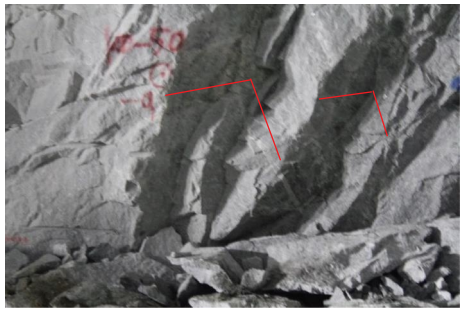

Figure 23: Damage of the top arch joint of the upstream side wall in the K0 + 100 m of the pilot tunnel in the main powerhouse.

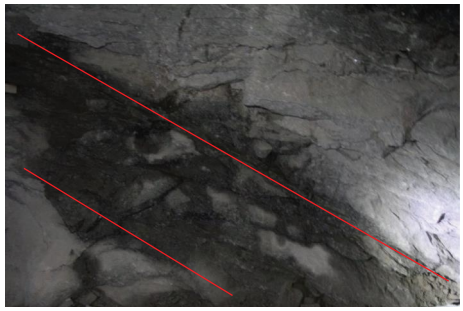

Figure 24: K0 + 135 lamprophyre vein of the main powerhouse.

Figure 25: Fault slip-type rockburst on the upstream side of the pilot tunnel in K0 + 70 m of the main transformer chamber.

chamber, and there are large pieces of caving. The rockburst at this place is controlled by a group of structural planes 220°∠30° with spacing of 3 m, and moderate-strength fault slip-type rockburst occurs here, as shown in Figure 26.

During the investigation of the main transformer chamber, it is found that the deformation and failure of rock mass under high ground stress present a gradual failure process. After the blasting excavation is completed, the stress redistribution on the surface of the chamber is completed rapidly, accompanied by dense splitting sound, forming a plate-shaped splitting parallel to the shape of the chamber. Initial deformation and failure will occur within the section of the chamber and plate-shaped falling blocks will appear on the top arch surface. Block dumping and spalling will appear on the side walls on both sides, and there is plate spalling near the spandrels and the lower part of the side wall. These usually occur within a few hours after excavation. In the first few hours, many fissures tending to the free face

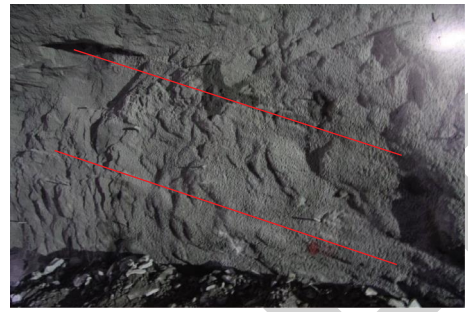

Figure 26: Wedge failure of side wall and arch shoulder in K0 + 10 m of the main transformer room downstream.

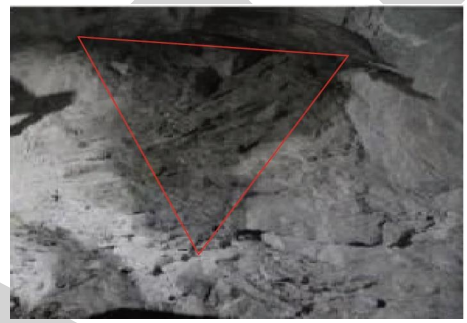

Figure 27: Destruction of the deep and large structural plane in K0 + 545 m of the tailrace surge chamber pilot hole.

will be formed around the tunnel. In 2 to 3 days, these fissures will continue to expand, and, with the expansion of the fissures, there will be occasional damage and dangerous blocks. In the following one week, there will be occasional falling blocks at the spandrel of the tunnel, and further damage will occur near the spandrel during the further forward blasting excavation. There are two reasons: The first reason is blasting disturbance. The second reason is that as the tunnel face moves forward, the stress will be adjusted again at a certain distance from the tunnel face. The damage usually presents V-shaped pit or V-shaped strip, and the blasting influence range is generally about 30 m behind the tunnel face, indicating that the disturbance induces the fault slip-type rockburst.

5.3. Investigation of Fault Slip-Type Rockburst in the Tailrace Chamber. As shown in Figure 27, the downstream side wall at K0 + 545 m of tailrace chamber is affected by the structural plane (220°∠ 68°), where a large wedge-shaped blasting pit is formed and moderate strength fault slip-type rockburst occurs. The spandrel on the downstream side at the pilot tunnel K0 + 540 m in the tailrace chamber forms a wedge-shaped rockburst cavity, which is 1 m deep, 5 m high, and 5 m long, with water seepage. The structural plane 245°∠45° is the downward sliding plane of wedge-shaped block. This group of structural planes are relatively developed, and the downstream side failure is mostly caused by fault slip-type rockburst under the action of this group of structural planes.

The pilot tunnel K0 + 530~K0 + 570 m in the tailrace chamber is affected by the structural plane 220°~250°∠

Figure 28: Wedge cavity of arch shoulder in K0 + 540 m of the tailrace surge chamber pilot hole downstream.

35–55°, and the upstream and downstream side walls are deformed and damaged under the coordinated control of structure and stress. The upstream side is an inverted sill, and this group of structural planes at the downstream side form the natural shear outlet of the unloading structural plane blocks. Extrusion fracture zone can be seen on the footwall of the fracture zone of the downstream side wall in the pilot tunnel K0 + 540 m of the tailrace chamber, with obvious dislocation marks, as shown in Figure 28.

To sum up, first of all, the occurrence of the fault slip-type rockburst is because the surrounding rock contains the dominant structural plane, and the rock blocks on the structural plane have a tendency to slide towards the free face. Before the rockburst occurs, a large amount of energy is accumulated in the surrounding rock, and the elastic strain energy is suddenly released under the action of excavation and unloading. The elastic strain energy accumulated in the rock mass is greater than the energy required for the slip of the structural plane and the generation of cracks in the rock mass. The excess elastic strain energy drives the rock blocks on the structural plane to slide down rapidly in the form of kinetic energy, accompanied by vibrations. Therefore, the fault slip-type rockburst occurs. At the same time, after the excavation and unloading, there is no rock block caving in the surrounding rock, but there are potential blocks sliding towards the free face in the surrounding rock. Under the action of dynamic disturbance, the friction force of the structural plane changes from static to dynamic, that is, ultralow friction effect. When the dynamic friction force is less than the shear force of the structural plane, the rock block slip leads to the instability and collapse of rock mass blocks, resulting in slip-type rockburst.

6. Conclusions

Taking the underground cavern of Shuangjiangkou Hydropower Station as the research object, the frequency and location of microseismic events in the underground powerhouse are collected through the microseismic monitoring system, and the characteristics of microseismic events are analyzed to explore the internal relationship between rockbursts and microseismic events. The risk level of rockbursts is predicted by microseismic monitoring of the change of b value. The occurrence mechanism of fault slip-type rockburst in the underground cavern of Shuangjiangkou Hydropower Station is explored in combination with the on-site rockburst situation. The main conclusions are as follows:

(1) The underground caverns of Shuangjiangkou Hydropower Station mainly have slight rockbursts, with less moderate rockbursts and no strong rockbursts. Microseismic events are active at the structural plane of the main powerhouse, with a high probability of rockburst. The microseismic events are closely related to the excavation activities; the stronger the unloading or disturbance, the greater the risk of rockburst. On the contrary, optimizing the construction scheme and strengthening the support can reduce the number and the magnitude of microseismic events. It is consistent with the occurrence of rockburst on-site.

(2) The b value of microseismic activity can reflect the activities of microseismic events with different magnitudes, and the change of b value can reflect the risk level of rockburst. It can be used as an important index to reflect the overall stability of regional surrounding rock. The smaller the b value of microseismic events is, the more events with large magnitudes are and the greater the possibility of rockburst is.

(3) Fault slip-type rockburst is mainly affected by structural plane. Faults and large structural plane are easy to induce moderate-strength rockburst. Fault slip-type rockburst is mainly characterized by the slip of large blocks of surrounding rock, forming a V-shaped blasting pit or wedge-shaped blasting pit. It can be seen that the structural plane is exposed, and the failure is accompanied by a blast cracking sound, which is more serious than the strain-type rockburst.

(4) Fault slip-type rockburst accumulates large elastic strain energy under the action of high stress. Due to the existence of structural plane, the rock mass on the structural plane tends to slide towards the free face. Under the action of excavation unloading or mechanical disturbance, the rock mass on the structural plane suddenly slips, accompanied by the release of strain energy; that is, the fault slip-type rockburst occurs.

Data Availability

The data used to support the findings of this study are included within the article.

Conflicts of Interest

The authors declare that they have no conflicts of interest.

Acknowledgments

The authors acknowledge the National Natural Science Foundation of China (42002275), Natural Science Foundation

of Zhejiang Province (LQ21D020001), and China Postdoctoral Science Foundation (2021M692319).

References

[1] J. S. Jia, "A technical review of hydro-project development in China," *Engineering*, vol. 2, no. 3, pp. 302–312, 2016.

[2] T. B. Zhao, M. l. Xing, W. Y. Guo, C. W. Wang, and B. Wang, "Anchoring effect and energy-absorbing support mechanism of large deformation bolt," *Journal of Central South University*, vol. 28, no. 2, pp. 572–581, 2021.

[3] C. Wang, R. Liu, Y. Jiang, G. Wang, and H. Luan, "Effect of shear-induced contact area and aperture variations on nonlinear flow behaviors in fractal rock fractures," *Journal of Rock Mechanics and Geotechnical Engineering*, 2022.

[4] G. L. Feng, B. R. Chen, Y. X. Xiao et al., "Microseismic characteristics of rockburst development in deep TBM tunnels with alternating soft-hard strata and application to rockburst warning: a case study of the Neelum-Jhelum hydropower project," *Tunnelling and Underground Space Technology*, vol. 122, Article ID 104398, 2022.

[5] G. L. Feng, X. T. Feng, B. R. Chen, Y. X. Xiao, and Y. Yu, "A microseismic method for dynamic warning of rockburst development processes in tunnels," *Rock Mechanics and Rock Engineering*, vol. 48, no. 5, pp. 2061–2076, 2015.

[6] M. Cai, H. Morioka, P. K. Kaiser et al., "Back-analysis of rock mass strength parameters using AE monitoring data," *International Journal of Rock Mechanics and Mining Sciences*, vol. 44, no. 4, pp. 538–549, 2007.

[7] Q. Yu, C. A. Tang, L. C. Li, G. Cheng, and L. X. Tang, "Study on rockburst nucleation process of deep-buried tunnels based on microseismic monitoring," *Shock and Vibration*, vol. 2015, Article ID 685437, 17 pages, 2015.

[8] F. Dai, B. Li, N. W. Xu, Y. Zhu, and P. Xiao, "Stability evaluation on surrounding rocks of underground powerhouse based on microseismic monitoring," *Shock and Vibration*, vol. 2015, Article ID 937181, 9 pages, 2015.

[9] Y. S. Li and C. Zhou, "Rockburst inducement mechanism and its prediction based on microseismic monitoring," *Geofluids*, vol. 2021, Article ID 4028872, 9 pages, 2021.

[10] X. L. Guo, "First-arrival picking for microseismic monitoring based on deep learning," *International Journal of Geophysics*, vol. 2021, Article ID 5548346, 14 pages, 2021.

[11] W. L. Zhang, T. H. Huo, C. Li, C. Wang, X. Qu, and C. Xin, "Characteristics of valuable microseismic events in heading face of an underground coal mine using microseismic system," *Shock and Vibration*, vol. 2021, Article ID 6683238, 10 pages, 2021.

[12] T. H. Ma, D. Y. Lin, C. A. Tang, K. P. Yadav, Z. Feng, and K. Ma, "Microseismic monitoring, positioning principle, and sensor layout strategy of rock mass engineering," *Geofluids*, vol. 2020, Article ID 8810391, 20 pages, 2020.

[13] Y. J. Wang, D. J. Lei, Y. Y. Zheng, and T. Ma, "Study on response characteristics of surrounding rock rupture microseismic events during coal roadway excavation," *Shock and Vibration*, vol. 2021, Article ID 9955994, 12 pages, 2021.

[14] Q. Jiang, X. T. Feng, T. B. Xiang, and G. S. Su, "Rockburst characteristics and numerical simulation based on a new energy index: a case study of a tunnel at 2,500 m depth," *Bulletin of Engineering Geology and the Environment*, vol. 69, no. 3, pp. 381–388, 2010.

[15] B. Li, Q. F. Ding, N. W. Xu, F. Dai, Y. Xu, and H. Qu, "Characteristics of microseismic b-value associated with rock mass large deformation in underground powerhouse caverns at different stress levels," *Journal of Central South University*, vol. 29, no. 2, pp. 693–711, 2022.

[16] Z. G. Yang, R. C. Yu, R. Guo, and L. Wang, "Application of microseismic monitoring to deep mines," *Chinese Journal of Rock Mechanics and Engineering*, vol. 27, no. 05, pp. 1066–1073, 2008.

[17] Y. C. Lei, G. He, and S. Y. Chen, "Method and technology of effective event extracting of dam concrete micro-seismic monitoring in Guanyinyan hydropower station," *Water Power*, vol. 43, no. 01, pp. 101–106, 2017.

[18] W. D. Zhang, T. H. Ma, C. A. Tang, and L. X. Tang, "Research on characteristics of rockburst and rules of microseismic monitoring at diversion tunnels in jinping ii hydropower station," *Chinese Journal of Rock Mechanics and Engineering*, vol. 33, no. 02, pp. 339–348, 2014.

[19] Z. P. Huang, S. Yan, and F. S. Liu, "Microseismic monitoring system of No. 4 construction adit of qinling water conveyance tunnel for hanjiang river to weihe river water transfer project and its engineering application," *Water Resources and Hydropower Engineering*, vol. 49, no. 9, pp. 102–110, 2018.

[20] S. B. Hu, "Application of microseismic monitoring and prediction rockburst technology in jinping diversion tunnel construction," *Sichuang Architecture*, vol. 49, no. 9, pp. 102–110, 2018.

[21] L. Tao, Y. L. Shi, and K. N. Dang, "Study on microseismic monitoring and early warning of rockburst in buried hydraulic tunnel," *Water Resources Planning and Design*, vol. 12, no. 04, pp. 126–131, 2020.

[22] N. W. Xu, T. Li, F. Dai, and P. W. Xiao, "Stability analysis on surrounding rock mass in underground caverns based on discrete element simulation and microseismic monitoring," *Journal of Sichun University*, vol. 48, no. 05, pp. 1–8, 2016.

[23] B. Li, F. Dai, N. W. Xu, and Y. G. Zhu, "Microseismic monitoring system and its engineering applications of deep-buried underground powerhouse," *Chinese Journal of Rock Mechanics and Engineering*, vol. 33, no. S1, pp. 3375–3383, 2014.

[24] F. Dai, B. Li, N. W. Xu, Y. L. Fan, and J. Xu, "Microseismic characteristic analysis of underground powerhouse at Baihetan hydropower station subjected to excavation," *Chinese Journal of Rock Mechanics and Engineering*, vol. 35, no. 04, pp. 692–703, 2016.

[25] A. Li, F. Dai, N. W. Xu, G. K. Gu, and K. Liu, "Failure mechanism and mode of surrounding rock of underground powerhouse at the right bank of Wudongde hydropower station subjected to excavation," *Chinese Journal of Rock Mechanics and Engineering*, vol. 36, no. 04, pp. 781–793, 2017.

[26] G. Wang, L. B. Song, X. Q. Liu, C. Y. Bao, M. Q. Lin, and G. J. Liu, "Shear fracture mechanical properties and acoustic emission characteristics of discontinuous jointed granite," *Rock and Soil Mechanics*, vol. 43, no. 06, pp. 1–13, 2022.

[27] A. Li, N. W. Xu, F. Dai et al., "Microseismic monitoring and large deformation forecasting research during excavation of underground powerhouse at Wudongde hydropower station," *Chinese Journal of Rock Mechanics and Engineering*, vol. 36, no. S2, pp. 4102–4112, 2017.

[28] Y. L. Wen, G. Q. Fang, and W. Z. Zhao, "Microseismic monitoring: bridging the gap between rock acoustic emission

and natural earthquakes," *Progress in Earthquake Sciences*, vol. 13, no. 09, p. 71, 2015.

[29] L. Song, G. Wang, X. Wang et al., "The influence of joint inclination and opening width on fracture characteristics of granite under triaxial compression," *International Journal of Geomechanics*, vol. 22, no. 5, Article ID 04022031, 2022.

[30] L. Hu, K. Ma, X. Liang, C. Tang, Z. Wang, and L. Yan, "Experimental and numerical study on rockburst triggered by tangential weak cyclic dynamic disturbance under true triaxial conditions," *Tunnelling and Underground Space Technology*, vol. 81, pp. 602–618, 2018.

[31] Y. Luo, G. Wang, X. Li et al., "Analysis of energy dissipation and crack evolution law of sandstone under impact load," *International Journal of Rock Mechanics and Mining Sciences*, vol. 132, Article ID 104359, 2020.